

Report Number 09/40

Stationary bumps in a piecewise smooth neural field model with synaptic depression

by

Zachary P Kilpatrick and Paul C. Bressloff



Oxford Centre for Collaborative Applied Mathematics
Mathematical Institute
24 - 29 St Giles'
Oxford
OX1 3LB
England

Manuscript submitted to
AIMS' Journals
Volume **X**, Number **0X**, XX **200X**

Website: http://AIMsciences.org

pp. **X–XX**

STATIONARY BUMPS IN A PIECEWISE SMOOTH NEURAL FIELD MODEL WITH SYNAPTIC DEPRESSION

Paul C Bressloff

Mathematical Institute
University of Oxford, 26-29 St. Giles'
Oxford, OX1 3LB, UK

Zachary P Kilpatrick

Department of Mathematics
University of Utah, 155 South 1400 East
Salt Lake City, UT 84112, USA

(Communicated by the associate editor name)

Abstract. **We analyze the existence and stability of stationary pulses or bumps in a one–dimensional piecewise smooth neural field model with synaptic depression. The continuum dynamics is described in terms of a nonlocal integrodifferential equation, in which the integral kernel represents the spatial distribution of synaptic weights between populations of neurons whose mean firing rate is taken to be a Heaviside function of local activity. Synaptic depression dynamically reduces the strength of synaptic weights in response to increases in activity. We show that in the case of a Mexican hat weight distribution, there exists a stable bump for sufficiently weak synaptic depression. However, as synaptic depression becomes stronger, the bump became unstable with respect to perturbations that shift the boundary of the bump, leading to the formation of a traveling pulse. The local stability of a bump is determined by the spectrum of a piecewise linear operator that keeps track of the sign of perturbations of the bump boundary. This results in a number of differences from previous studies of neural field models with Heaviside firing rate functions, where any discontinuities appear inside convolutions so that the resulting dynamical system is smooth. We also extend our results to the case of radially symmetric bumps in two–dimensional neural field models.**

1. **Introduction.** Continuum neural field models provide an important example of spatially extended excitable systems with nonlocal interactions. These models represent the large–scale dynamics of populations of neurons in terms of nonlinear integrodifferential equations whose associated integral kernels represent the spatial distribution of neuronal synaptic connections [1, 2, 3, 4, 5]. As in the case of nonlinear PDE models of diffusively coupled excitable systems [6], neural field models can exhibit a variety of coherent pulse–like structures including both stationary and traveling solitary pulses. Traveling pulses tend to occur when synaptic connections are predominantly excitatory and there is some form of slow local adaptation or

2000 *Mathematics Subject Classification.* Primary: 92; Secondary: 53C35.
Key words and phrases. Integrodifferential equations, neural field theory, traveling waves.

recovery [7], whereas stationary pulses occur in the presence of lateral inhibition [2, 8]. The formation of localized activity states can be used to model a number of neurobiological phenomena. For example, traveling pulses have been observed in disinhibited slice preparations [9, 10, 11] using voltage sensitive dyes and multiple electrodes. A second example is given by a delayed response task in which an animal is required to retain information of a sensory cue across a delay period between the stimulus and behavioral response. Physiological recordings in prefrontal cortex have shown that spatially localized groups of neurons fire during the recall task and then stop firing once the task has finished [12]. Thus persistent localized states of activity are thought to be neural correlates of spatial working memory.

The simplest example of a one–dimensional neural field model is the scalar equation [2]

$$\tau \frac{\partial u(x,t)}{\partial t} = -u(x,t) + \int_{-\infty}^{\infty} w(x-x')f(u(x',t))dx' + h(x,t). \tag{1}$$

The neural field $u(x,t)$ represents the local activity of a population of neurons at position x at time t, τ is a membrane or synaptic time constant, $h(x,t)$ represents an external input, and $w(x)$ is a synaptic weight distribution. We assume that w is a continuous function satisfying $w(-x) = w(x)$ and $\int_{-\infty}^{\infty} w(x) < \infty$. The nonlinearity f denotes an output firing rate function. A typical choice for f is a bounded, positive monotonic function such as the sigmoid

$$f(u) = \frac{1}{1+\mathrm{e}^{-\eta(u-\theta)}}. \tag{2}$$

with gain η and threshold θ. Most analytical studies of the existence and stability of spatially localized solutions of equation (1) and its generalizations have been obtained by taking the high–gain limit $\eta \to \infty$ such that f becomes a Heaviside function [2, 7, 8].

$$f(u) = H(u-\theta) = \begin{cases} 0 & \text{if } u < \theta \\ 1 & \text{if } u > \theta \end{cases} \tag{3}$$

It is then possible to establish existence of pulse solutions by explicit construction and to determine local stability in terms of an associated Evans function [13]. The latter is obtained by linearizing the neural field equations about the pulse solution. In the case of stationary pulses or bumps, local stability reduces to the problem of calculating the effects of perturbations at the bump boundary where $u(x) = \theta$.

Equation (1) was first analyzed in detail by Amari [2], who showed that in the case of a Heaviside function H and a homogeneous external input h, the network can support a stable stationary bump solution when the weight distribution $w(x)$ is given by a so–called Mexican hat function with the following properties:

(i) $w(x) > 0$ for $x \in [0, x_0)$ with $w(x_0) = 0$
(ii) $w(x) < 0$ for $x \in (x_0, \infty)$
(iii) $w(x)$ is decreasing on $[0, x_0]$
(iv) $w(x)$ has a unique minimum on $\mathbb{R}^+$ at $x = x_1$ with $x_1 > x_0$ and $w(x)$ strictly increasing on (x_1, ∞).

On the other hand, in the case of a purely excitatory network with $w(x)$ a positive, monotonically decreasing function, any bump solution is unstable and tends to break up into a pair of counterpropagating fronts. Following Amari's original analysis, Kishimoto and Amari [14] proved the existence of a stationary pulse for a smooth sigmoidal nonlinearity f rather than a Heaviside function using a fixed point

theorem. More recently, functional analytical techniques have been used to study stationary bump solutions for a general class of neural field models with smooth f, where the spatial domain is taken to be bounded rather than infinite [15]. The constructive approach based on the Heaviside function has also been generalized in a number of ways (see the review by Coombes [5]). These include more general weight distributions for which multiple bump states can arise [16, 17], inhomogeneous neural fields [18], two-dimensional bumps [19, 17, 20, 21], and weakly interacting bumps [22]. There has also been a lot of recent interest in neural field models with some form of local negative feedback. The inclusion of negative feedback is motivated by the fact that the scalar model given by equation (1) cannot support traveling pulse solutions in the absence of synaptic inhibition, which is inconsistent with what is observed in disinhibited slice experiments. [8]. Negative feedback is typically taken to be linear by analogy with the Fitzhugh-Nagumo equation [23], leading to a neural field model of the form [7, 8]

$$\tau \frac{\partial u(x,t)}{\partial t} = -u(x,t) + \int_{-\infty}^{\infty} w(x,x') f(u(x',t)) \mathrm{d}x' - v(x,t) + h(x,t), \quad (4)$$

$$\epsilon \frac{\partial v(x,t)}{\partial t} = \gamma u(x,t) - v(x,t). \quad (5)$$

The auxiliary field $v(x,t)$ represents a slow local negative feedback component with ϵ and γ determining the time constant and strength of the feedback, respectively. One of the interesting dynamical consequences of linear negative feedback is that the spectrum of the linear operator obtained by linearizing about a stationary bump solution can have complex–valued eigenvalues, thus providing a possible mechanism for the generation of spatially structured oscillations [20, 21, 24, 25].

In this paper we use the constructive approach to study the existence and stability of stationary bumps in a neural field model with a nonlinear form of negative feedback that represents the effects of synaptic depression. Synaptic depression is the process by which presynaptic resources such as chemical neurotransmitter or synaptic vesicles are depleted [26]. It can be incorporated into the scalar neural field model (1) by introducing a dynamic prefactor q in the nonlocal term according to [27, 28]

$$\tau \frac{\partial u(x,t)}{\partial t} = -u(x,t) + \int_{-\infty}^{\infty} q(x',t) w(x-x') f(u(x',t)) \mathrm{d}x', \quad (6a)$$

$$\frac{\partial q(x,t)}{\partial t} = \frac{1-q(x,t)}{\alpha} - \beta q(x,t) f(u(x,t)). \quad (6b)$$

The factor $q(x,t)$ can be interpreted as a measure of the fraction of available presynaptic resources, which are depleted at a rate βf [29, 30], and are recovered on a timescale specified by the constant α (experimentally shown to be 200-800ms [31, 32, 29]). If we assume that the strength of a synapse is reduced by a factor $\kappa = 0.05 - 0.9$ of its maximal value in response to a sustained input of rate $f = 1$ [31], then a simple steady–state calculation shows that $\beta \approx (1-\kappa)/(\kappa\alpha) \approx 0.0001 - 0.1$ $(\mathrm{ms})^{-1}$ for the given range of values of α. In previous work we focused on the role of synaptic depression in generating spatially structured oscillations in one-dimensional [27] and two-dimensional [28] excitatory neural networks with continuous firing rate functions. In the high–gain limit oscillatory solutions no longer exist but stationary and traveling wave solutions can be constructed. However, the presence of a Heaviside function in the dynamics of the synaptic depression variable

means that the resulting dynamical system is piecewise smooth, which considerably complicates the stability analysis. Indeed, a preliminary analysis of bump stability suggests that considerable care has to be taken in evaluating terms arising from perturbations of the bump boundary [27]. Here we present a more detailed analysis of stationary bumps, both in one–dimensional and two–dimensional neural field models with synaptic depression, which explicitly handles the piecewise nature of the dynamics.

2. **Existence and stability of bumps in the scalar equation.** It is useful to begin by briefly reviewing the analysis of bumps in the scalar neural field equation (1) with $f(u) = H(u-\theta)$ and $h \equiv 0$. Equilibrium solutions of equation (1) satisfy

$$U(x) = \int_{-\infty}^{\infty} w(x-x')H[U(x')-\theta]dx'. \tag{7}$$

Let $R[U] = \{x|U(x) > \theta\}$ be the region over which the field is excited or superthreshold. Equation (7) can then be rewritten as

$$U(x) = \int_{R[U]} w(x-x')dx'. \tag{8}$$

Exploiting the fact that any solution can be arbitrarily translated so that it is

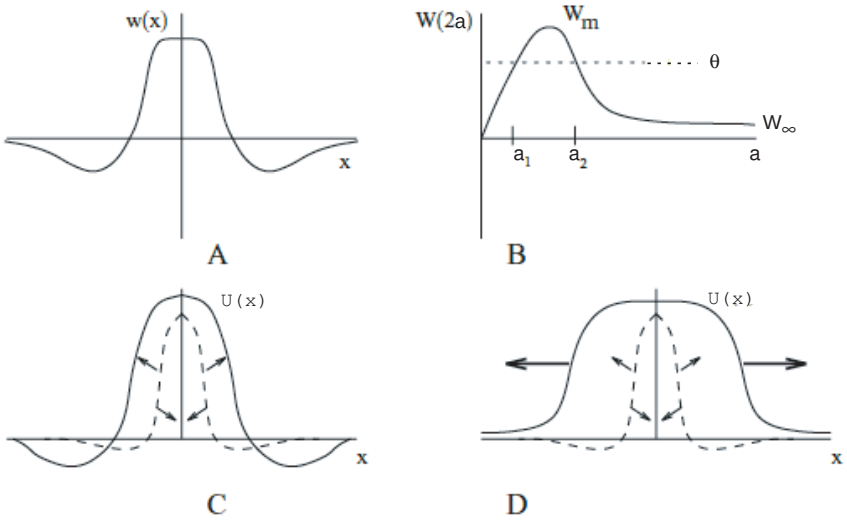

FIGURE 1. Construction of a solitary pulse in the Amari model. (a) A Mexican hat weight distribution w. (b) Integral $W(x)$ of $w(x)$. Horizontal line shows the threshold θ whose intersections with $W(2a)$ determine the allowed stationary pulse solutions. If $W_\infty < \theta < W_m$ then there exists an unstable bump of half–width a_1 and a stable bump of half–width a_2. On the other hand, if $0 < \theta < W_\infty$ then there only exists an unstable bump.(c) Unstable bump (broken) acting as a separatrix between a stable bump and the uniform rest state. (d) For $0 < \theta < W_\infty$ the unstable bump acts as a separatrix between a wavefront and the rest state. [Adapted from [3]]

centered at the origin, we define a stationary pulse solution of half–width a to be one that is excited over the interval $(-a, a)$. Let

$$W(x) = \int_0^x w(y)dy \tag{9}$$

and

$$W_m = \max_{x>0} W(x), \quad W_\infty = \lim_{x\to\infty} W(x) \tag{10}$$

such that $W(0) = 0$ and $W(-x) = -W(x)$. For a bump of half–width a, equation (8) reduces to the form

$$U(x) = W(a + x) - W(x - a). \tag{11}$$

Since $U(\pm a) = \theta$ by definition, we obtain the following necessary condition for the existence of a bump:

$$W(2a) = \theta. \tag{12}$$

This condition is also sufficient for a Mexican hat weight distribution [2]. It will be shown below that a bump is stable provided the condition $W'(2a) < 0$ is satisfied. The existence and stability of activity bumps for a given θ can thus be determined graphically as illustrated in figure 1(b). For a certain range of values of $\theta > 0$ one finds bistability between a stable bump and a uniform rest state, $U(x) = 0$ for all $x \in \mathbb{R}$, with an unstable bump acting as a separatrix between these two solutions.

The linear stability of a stationary pulse can be determined by setting $u(x, t) = U(x) + \psi(x)e^{\lambda t/\tau}$ and expanding to first order in ψ [8, 20, 13]. This leads to the eigenvalue equation

$$(\lambda + 1)\psi(x) = \int_{-\infty}^{\infty} w(x - x')\delta(U(x'))\psi(x')dx'. \tag{13}$$

Using the identity

$$\delta(U(x)) = \left(\frac{\delta(x - a)}{|U'(a)|} + \frac{\delta(x + a)}{|U'(-a)|} \right), \tag{14}$$

and setting $|U'(a)| = U'(-a) = \gamma^{-1}$, we have

$$(\lambda + 1)\psi(x) = \gamma \left(w(x - a)\psi(a) + w(x + a)\psi(-a) \right). \tag{15}$$

There are two types of solution to this equation. The first consist of solutions $\psi(x)$ that vanish at $x = \pm a$ so that $\lambda = -1$. This defines the essential spectrum and does not contribute to any instabilities. The second class of solution, which generates the discrete spectrum, is obtained by setting $x = \pm a$ in the eigenvalue equation,

$$(\lambda + 1)\psi(a) = \gamma \left(w(0)\psi(a) + w(2a)\psi(-a) \right) \tag{16}$$

$$(\lambda + 1)\psi(-a) = \gamma \left(w(-2a)\psi(a) + w(0)\psi(-a) \right). \tag{17}$$

This has the solutions $\psi(-a) = \pm\psi(a)$ with corresponding eigenvalues

$$\lambda_\pm = -1 + \gamma(w(0) \pm w(2a)). \tag{18}$$

Finally, using the fact that $\gamma^{-1} = w(0) - w(2a)$ we deduce that $\lambda_- = 0$ (reflecting the translation invariance of the system) and $\lambda_+ = 2\gamma w(2a)$. Thus the bump is stable provided that $w(2a) = W'(2a) < 0$.

Note that the discrete spectrum is determined completely in terms of the perturbations $\psi(\pm a)$. This explains why it is also possible to analyze the stability of the bumps by restricting attention to the effects of perturbations at the boundaries of the activity bump as originally formulated by Amari [2]. In particular, if $\Delta_+(t)$

denotes a perturbation in the position of the right–hand edge of the bump so that $u(x,t)=\theta$ at $x=x+a+\Delta_+(t)$, then

$$\begin{aligned}\theta &= U(a+\Delta_+(t))+\psi(a+\Delta_+(t),t)\\ &= U(a)+U'(a)\Delta_+(t)+\psi(a,t)+\mathcal{O}(\Delta^2),\end{aligned}$$

that is,

$$\Delta_+(t)=\gamma\psi(a,t) \tag{19}$$

since $U(a)=\theta$ and $U'(a)=-\gamma^{-1}$. Similarly, the shift $\Delta_-(t)$ of the left–hand edge satisfies

$$\Delta_-(t)=-\gamma\psi(-a,t). \tag{20}$$

It follows that the eigenmode $\psi(-a,t)=\psi(a,t)$ generates a uniform expansion or contraction of the bump ($\Delta_-=-\Delta_+$) whereas $\psi(-a,t)=-\psi(a,t)$ generates a shift in the center of the bump ($\Delta_-=\Delta_+$).

3. **Piecewise–smooth network with synaptic depression.** In this section, we analyze the existence and stability of stationary bumps in a one–dimensional neural field model with synaptic depression, whose dynamics is described by equation (6) with f given by the Heaviside function (3). In contrast to the scalar equation, the dynamics is now only piecewise smooth due to the presence of the Heaviside function in the dynamical equation for the depression variable $q(x,t)$. In the following we set the time constant $\tau=1$ which sets the unit of time to be of the order $10ms$.

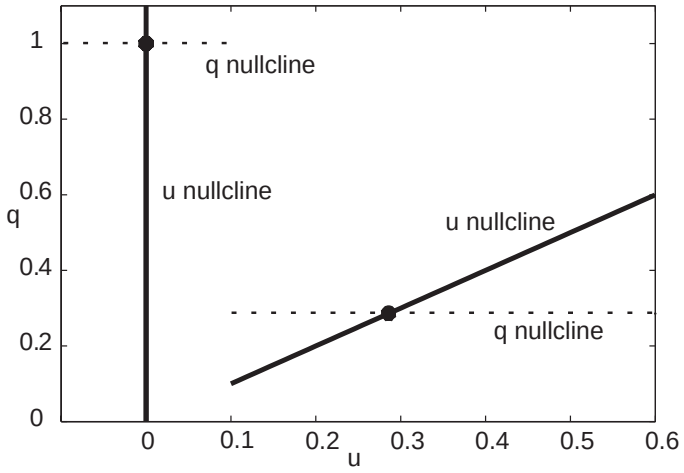

FIGURE 2. Phase plane plot of the space-clamped system (21) in the case $\theta<1/(1+\alpha\beta)$ for which there exist two stable fixed points. Parameters are $\alpha=50$, $\beta=0.05$, and $\theta=0.1$.

3.1. **Phase–plane analysis.** Let us first consider the corresponding space–clamped system in which solutions are restricted to be spatially uniform:

$$\begin{aligned}\dot{u}(t) &= -u(t)+q(t)H(u(t)-\theta),\\ \alpha\dot{q}(t) &= 1-q(t)-\alpha\beta q(t)H(u(t)-\theta).\end{aligned} \tag{21}$$

In order to calculate equilibria of (21), we consider the possible solutions on the two domains of the step function $H(u-\theta)$. We find that there is always a low activity

or Down state on the lower domain ($u < \theta$) for $\theta > 0$ such that $(u, q) = (0, 1)$. The stability of this Down state is determined by the eigenvalues of the Jacobian

$$\mathcal{J}(0,1) = \begin{pmatrix} -1 & 0 \\ 0 & -1/\alpha \end{pmatrix} \tag{22}$$

and is therefore stable since $\alpha > 0$. In the upper domain ($u > \theta$), an equilibrium is given by the system

$$0 = -u + q, \tag{23}$$

$$0 = (1 - q)/\alpha - \beta q, \tag{24}$$

implying a fixed point $(u,q) = (1/(1 + \alpha\beta),\ 1/(1 + \alpha\beta))$ will exist, provided $\theta < 1/(1 + \alpha\beta)$. Its stability is determined by the eigenvalues of the Jacobian

$$\mathcal{J}(u,q) = \begin{pmatrix} -1 & 1 \\ 0 & -(1/\alpha + \beta) \end{pmatrix}, \tag{25}$$

which guarantees that such an Up state is always stable. Therefore, we have a bistable system as long as $\theta < 1/(1 + \alpha\beta)$, as pictured in Fig. 2. However, if $\theta > 1/(1 + \alpha\beta)$, only the Down state exists, which physically means that in this case synaptic depression curtails recurrent excitation to the point that no sustained activity is possible. In the special case $\theta = 1/(1 + \alpha\beta)$, an equilibrium exists at $u = q = \theta$, provided that we take $H(0) = 1$. However, the piecewise smooth nature of the dynamics needs to be taken into account in order to determine the stability of the fixed point. That is, the fixed point is stable with respect to perturbations $\delta u > 0$ but unstable with respect to perturbations $\delta u < 0$. Thus, there does not exists a unique linear operator whose spectrum determines local stability. While this special case is non-generic in the space–clamped system, it foreshadows potential problems in the study of the stability of spatially structured solutions of the full system (6). This is due to the fact that one has to consider perturbations at threshold crossing points x where $u(x, t) = \theta$.

3.2. **Existence of 1D bumps.** Following our analysis of the scalar equation, a stationary bump solution $(U(x), Q(x))$ with associated excited region $R[U] = (-a, a)$ satisfies the pair of equations

$$U(x) = \int_{-a}^{a} Q(x')w(x - x')\mathrm{d}x', \tag{26}$$

$$Q(x) = 1 - \frac{\alpha\beta}{1 + \alpha\beta} H(U(x) - \theta). \tag{27}$$

Substituting equation (27) into (26) yields

$$U(x) = \frac{1}{1 + \alpha\beta}[W(x + a) + W(x - a)], \tag{28}$$

which is identical to the scalar case modulo a constant scale factor. As a simple example, consider a Mexican hat distribution given by the difference–of–exponentials

$$w(|x - x'|) = \mathrm{e}^{-|x-x'|} - A\mathrm{e}^{-|x-x'|/\sigma}. \tag{29}$$

Substituting the weight function (29) into the steady state solution for $U(x)$ and evaluating the integral yields

$$U(x) = \frac{1}{(1 + \alpha\beta)} \begin{cases} 2\sinh a\mathrm{e}^{-x} - 2A\sigma \sinh(a/\sigma)\mathrm{e}^{-x/\sigma}, & x > a, \\ 2 - 2\mathrm{e}^{-a}\cosh x - 2A\sigma[1 - \mathrm{e}^{-a/\sigma}\cosh(x/\sigma)], & |x| < a, \\ 2\sinh a\mathrm{e}^{x} - A\sigma \sinh(a/\sigma)\mathrm{e}^{x/\sigma}, & x < -a. \end{cases}$$

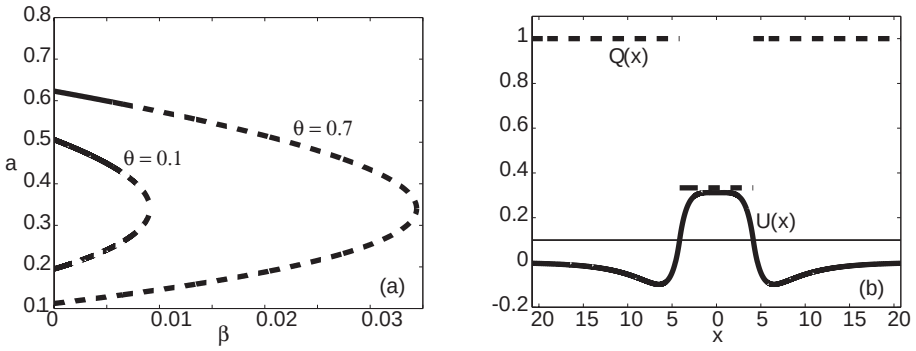

FIGURE 3. One–dimensional bumps. (a) Plots relating bump width a to amplitude of synaptic depression β for different values of θ using equation (30). Stable (unstable) bumps lie on the solid (broken) curve. For values of β beyond each curve's vertical asymptote, no bumps exist at that particular value of θ. Other parameter values are $A = 0.6$, $\sigma = 4$, $\alpha = 20$. (b) Bump profile when $\theta = 0.1$.

Applying the threshold conditions $U(\pm a) = \theta$, we arrive at an implicit expression relating the bump half–width a to all other parameters[1]:

$$\frac{1}{(1+\alpha\beta)}\left[1-\mathrm{e}^{-2a}-A\sigma(1-\mathrm{e}^{-2a/\sigma})\right] \quad = \quad \theta. \tag{30}$$

The transcendental equation (30) can be solved numerically using a root finding algorithm. The variation of pulse width with the parameters θ and β is shown in Figure 3; the stability of the bumps is calculated below.

3.3. **Stability of 1D bumps.** In the case of the scalar equation (1) it was possible to determine the local stability of a stationary bump by formally differentiating the Heaviside firing rate function inside the convolution integral, which is equivalent to differentiating with respect to the locations of the bump boundary. This is no longer possible for the neural field system (6), since the steady-state depression variable $Q(x)$ is a discontinuous function of x, reflecting the piecewise smooth nature of the depression dynamics. Formally Taylor expanding equations (6) about a bump solution in order to determine local stability of the bump requires prescribing $Q(x)$ on the bump boundary. The resulting stability conditions are necessary but not sufficient, that is, they underestimate the effectiveness of synaptic depression in destabilizing a bump [27]. Here we present a more rigorous treatment of local stability that explicitly takes into account the piecewise smooth nature of the dynamics.

[1]These threshold–crossing conditions are necessary but not sufficient for existence of a bump. A rigorous proof of existence, which establishes that activity is superthreshold everywhere within the domain $|x| < a$ and subthreshold for all $|x| > a$, has not been obtained except in special cases [2]. However, it is straightforward to check numerically that these conditions are satisfied.

Let us set $u(x,t) = U(x) + \psi(x,t)$ and $q(x,t) = Q(x) + \varphi(x,t)$. Substituting into the full system (6) and imposing the stationary bump solutions (26) and (27) gives

$$\begin{aligned}\frac{\partial \psi(x,t)}{\partial t} &= -\psi(x,t) \\ &\quad + \int_{-\infty}^{\infty} w(x-x')Q(x')\left[H(U(x')+\psi(x',t)-\theta) - H(U(x')-\theta)\right]\mathrm{d}x' \\ &\quad + \int_{-\infty}^{\infty} w(x-x')\varphi(x',t)H(U(x')+\psi(x',t)-\theta)\mathrm{d}x' \qquad (31)\\ \frac{\partial \varphi(x,t)}{\partial t} &= -\frac{\varphi(x,t)}{\alpha} - \beta Q(x)\left[H(U(x)+\psi(x,t)-\theta) - H(U(x)-\theta)\right] \\ &\quad -\beta\varphi(x,t)H(U(x)+\psi(x,t)-\theta). \qquad (32)\end{aligned}$$

Following our analysis of the scalar equation (1), denote the perturbations of the bump boundary by $\Delta_\pm(t)$ such that

$$u(a+\Delta_+(t),t) = u(-a+\Delta_-(t),t) = \theta$$

for all $t > 0$. Introducing the modified field

$$\Phi(x,t) = \int_{-a+\Delta_-(t)}^{a+\Delta_+(t)} w(x-x')\varphi(x',t)\mathrm{d}x', \qquad (33)$$

and convolving equation (32) with the weight function $w(x)$ between $-a+\Delta_-(t)$ and $a+\Delta_+(t)$ gives

$$\begin{aligned}\frac{\partial \psi(x,t)}{\partial t} &= -\psi(x,t) + \Phi(x,t) \\ &\quad + \int_{-a+\Delta_-(t)}^{a+\Delta_+(t)} w(x-x')Q(x')\mathrm{d}x' - \int_{-a}^{a} w(x-x')Q(x')\mathrm{d}x' \qquad (34)\\ \frac{\partial \Phi(x,t)}{\partial t} &= -\left(\alpha^{-1}+\beta\right)\Phi(x,t) \qquad (35)\\ &\quad -\beta\int_{-a+\Delta_-(t)}^{a+\Delta_+(t)} w(x-x')Q(x')\left[H(U+\psi-\theta) - H(U-\theta)\right]\mathrm{d}x'.\end{aligned}$$

So far we have not made any approximations. We now "linearize" equations (34) and (35) by only keeping terms having a magnitude that is first order in the perturbations $\psi, \Phi, \Delta_\pm$. However, it is important to keep track of the signs of $\Delta_\pm$ when approximating the various integrals, since the stationary solution $Q(x)$ is discontinuous at the bump boundary. For example,

$$\begin{aligned}\int_a^{a+\Delta_+} w(x-x')Q(x')\mathrm{d}x' &\approx \Delta_+ \lim_{\Delta_+\to 0} w(x-a-\Delta_+)Q(a+\Delta_+) \\ &= \Delta_+ \, w(x-a)G(\Delta_+) \qquad (36)\end{aligned}$$

and

$$\begin{aligned}\int_{-a+\Delta_-}^{-a} w(x-x')Q(x')\mathrm{d}x' &\approx -\Delta_- \lim_{\Delta_-\to 0} w(x+a-\Delta_-)Q(-a+\Delta_-) \\ &= -\Delta_- \, w(x+a)G(-\Delta_-), \qquad (37)\end{aligned}$$

where G is the step function

$$G(\Delta) = \begin{cases} 1 & \text{if } \Delta > 0 \\ (1+\alpha\beta)^{-1} & \text{if } \Delta < 0 \end{cases}. \qquad (38)$$

Similarly, the integral on the right–hand side of equation (35) can be approximated by the expression

$$\Delta_+(t)w(x-a)G(\Delta_+)H(\Delta_+) - \Delta_-(t)w(x+a)G(-\Delta_-)H(-\Delta_-). \tag{39}$$

Finally, having expanded the various integrals to first order in the perturbations, we can use equations (19) and (20) to obtain the following system of equations:

$$\begin{aligned}\frac{\partial \psi(x,t)}{\partial t} &= -\psi(x,t) + \Phi(x,t) + \gamma w(x+a)\psi(-a,t)G(\psi(-a,t)) \\ &\quad +\gamma w(x-a)\psi(a,t)G(\psi(a,t))\end{aligned} \tag{40}$$

$$\begin{aligned}\frac{\partial \Phi(x,t)}{\partial t} &= -\left(\alpha^{-1}+\beta\right)\Phi(x,t) \\ &\quad -\beta\gamma w(x+a)\psi(-a,t)G(\psi(-a,t))H(\psi(-a,t)) \\ &\quad -\beta\gamma w(x-a)\psi(a,t)G(\psi(a,t))H(\psi(a,t)).\end{aligned} \tag{41}$$

Here

$$\gamma^{-1} = U'(-a) = -U'(a) = \frac{w(0)-w(2a)}{1+\alpha\beta}. \tag{42}$$

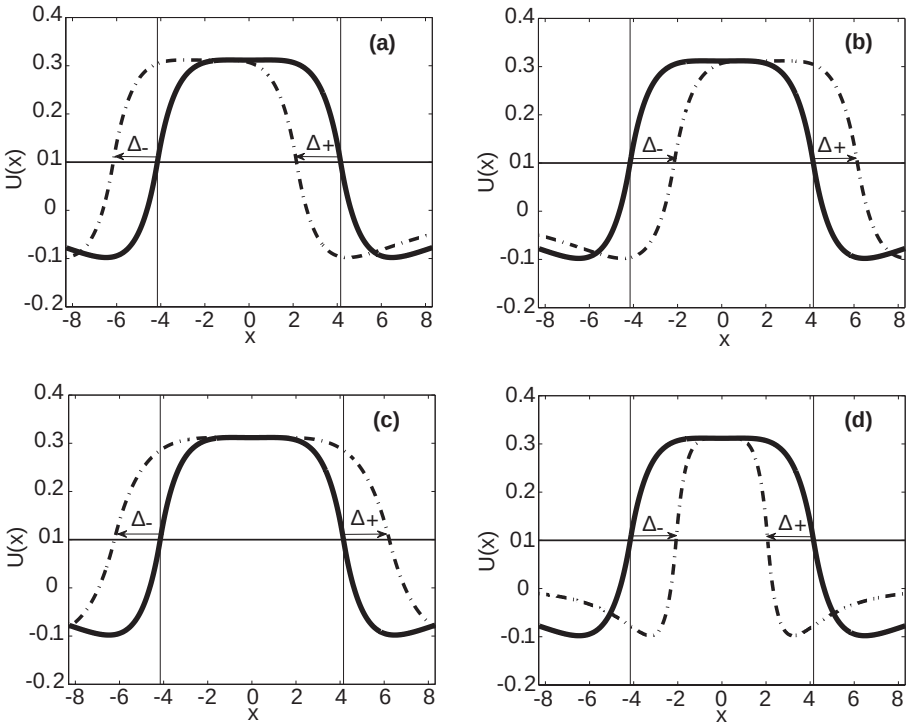

FIGURE 4. Illustration of different eigenmodes for one–dimensional bump perturbations.

Equations (40) and (41) imply that the local stability of a stationary bump solution depends on the spectral properties of a piecewise linear operator. However,

one can obtain a simpler spectral problem under the ansatz that the perturbations $\psi(\pm a,t)$ (or equivalently $\Delta_\pm(t)$) do not switch sign for any time t. In other words, we assume that equations (40) and (41) have separable solutions of the form $(\psi(x,t),\Phi(x,t)) = \mathrm{e}^{\lambda t}(\psi(x),\Phi(x))$, where λ is real. Under this assumption, the step functions H,G are time–independent so that there is a common factor $\mathrm{e}^{\lambda t}$ that cancels everywhere. We thus obtain an eigenvalue equation for λ of the form

$$\begin{aligned}(\lambda+1)\psi(x) &= \gamma w(x+a)\psi(-a)G(\psi(-a))\left(1-\frac{\beta H(\psi(-a))}{\lambda+\alpha^{-1}+\beta}\right)\\ &\quad+\gamma w(x-a)\psi(a)G(\psi(a))\left(1-\frac{\beta H(\psi(a))}{\lambda+\alpha^{-1}+\beta}\right).\end{aligned}\tag{43}$$

One particular class of solutions to equation (43) consists of functions $\psi(x)$ that vanish on the boundary, $\psi(\pm a)=0$, such that $\lambda=-1$. This determines the essential spectrum, since $\lambda=-1$ has infinite multiplicity, and does not contribute to any instabilities. There are then four other classes of solution to equation (43): (i) $\psi(-a)>0$ and $\psi(a)<0$; (ii) $\psi(-a)<0$ and $\psi(a)>0$; (iii) $\psi(-a)>0$ and $\psi(a)>0$; (iv) $\psi(-a)<0$ and $\psi(a)<0$. In the special case $|\psi(a)|=|\psi(-a)|$, the four types of perturbation correspond, respectively, to a leftward shift, a rightward shift, an expansion, and a contraction of the stationary bump solution. Figure 4 visualizes each of these cases for $\psi(x)$. If $|\psi(a)|\neq|\psi(-a)|$ then we have a mixture of these basic transformations. For example if $\psi(-a)>|\psi(a)|$ in case (i), then the perturbation is a mixture of a leftward shift and a bump expansion.

(i) $\psi(\pm a)\lesseqgtr 0$: In this case equation (43) becomes

$$\begin{aligned}\left(\lambda+\alpha^{-1}+\beta\right)(\lambda+1)\psi(x) &= \gamma w(x+a)\psi(-a)\left(\lambda+\alpha^{-1}\right)\\ &\quad+\gamma w(x-a)\psi(a)\frac{\lambda+\alpha^{-1}+\beta}{1+\alpha\beta}\end{aligned}\tag{44}$$

Setting $x=\pm a$ then yields the matrix equation

$$\begin{aligned}&\begin{pmatrix}\Gamma_\beta(\lambda)-\gamma w(0)\left(\lambda+\alpha^{-1}\right) & -\gamma\left(\lambda+\alpha^{-1}\right)w(2a)\\ -\gamma\left(\lambda+\alpha^{-1}\right)w(2a) & \Gamma_\beta(\lambda)-\gamma w(0)\left(\lambda+\alpha^{-1}\right)\end{pmatrix}\begin{pmatrix}\psi(-a)\\ \psi(a)\end{pmatrix}\\ &\qquad=-\frac{\gamma\alpha\beta\lambda}{1+\alpha\beta}\begin{pmatrix}w(2a)\psi(a)\\ w(0)\psi(a)\end{pmatrix},\end{aligned}\tag{45}$$

where

$$\Gamma_\beta(\lambda) = \left(\lambda+\alpha^{-1}+\beta\right)(\lambda+1).$$

The eigenvalues are determined by requiring that the determinant of the above matrix vanishes, which yields a quartic equation for λ. It is straightforward to show that there exists a zero eigenvalue $\lambda=0$ with corresponding eigenmode $\psi(-a)=-\psi(a)>0$, which represents a leftward shift. The existence of a zero eigenvalue reflects the translation invariance of the full system (6). In order to calculate any other eigenvalues, we assume that $\beta\ll 1$ (which is consistent with physiological values for the depletion rate of synaptic depression [29, 30]) and carry out a perturbation expansion in β. That is, we write $\psi(\pm a)=\psi_0^\pm+\beta\psi_1^\pm+\ldots$ and $\lambda=\lambda_0+\beta\lambda_1+\ldots$. First, setting $\beta=0$ in equation (45) shows that the lowest order solution (consistent with the fact that $\psi(\pm a)$ have opposite sign) is $\psi_0^-=-\psi_0^+$ with $\lambda_0=0,-\alpha^{-1}$. The zero eigenvalue solution persists when $\beta>0$, whereas the other solution picks up $\mathcal{O}(\beta)$ corrections. However, these do not lead to an instability,

at least for sufficiently small β. The corresponding eigenmode now consists of a combination of a leftward shift and a bump expansion or contraction.

(ii) $\psi(\pm a) \gtrless 0$: As expected from the reflection symmetry of the original system (6) when $w(x)$ is an even function, the spectrum associated with rightward shifts is identical to that of leftward shifts.

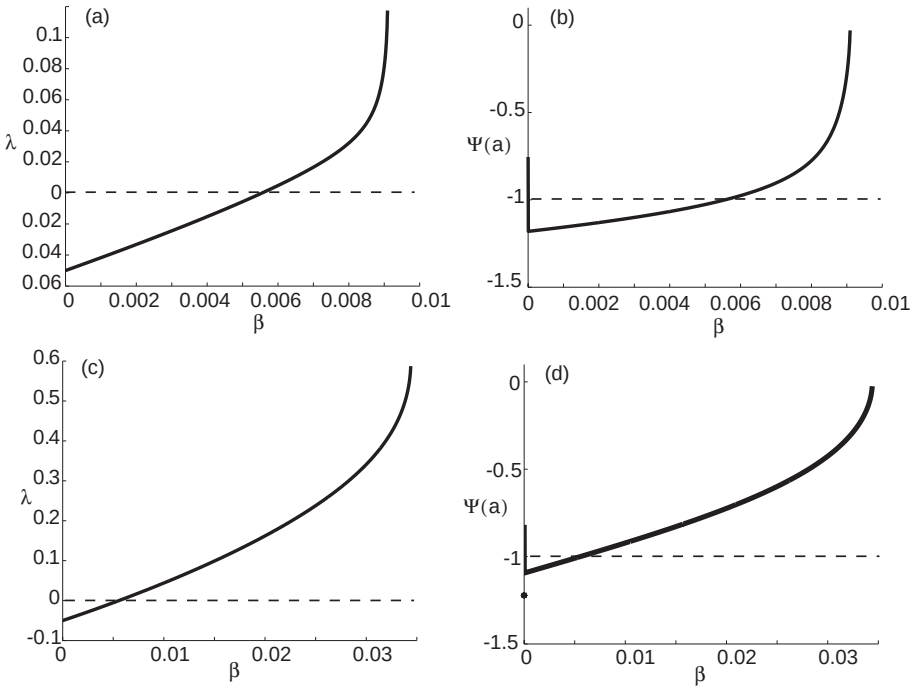

FIGURE 5. Stability of a stationary bump with respect to shift perturbations (cases (i) and (ii)). (a) Nonzero eigenvalue when $\theta = 0.1$ for various β. Bump destabilizes under shifts for sufficiently large β. (b) Corresponding plot of the ratio $\Psi(a) = \psi(a)/\psi(-a)$ for a leftward shift and $\theta = 0.1$. As β increases, the ratio approaches zero, implying the perturbation is a combination of a pure shift and an expansion. (c) Nonzero eigenvalue when $\theta = 0.07$ for various β. (d) Corresponding plot of the ratio $\Psi(a) = \psi(a)/\psi(-a)$ for a leftward shift and $\theta = 0.07$. Other parameters are $A = 0.6$, $\sigma = 4$, $\alpha = 20$. Results are the same for a rightward shift on exchanging $x = -a$ and $x = a$.

(iii) $\psi(\pm a) > 0$: In this case equation (43) becomes

$$\begin{aligned}\left(\lambda + \alpha^{-1} + \beta\right)(\lambda + 1)\psi(x) &= \gamma w(x+a)\psi(-a)\left(\lambda + \alpha^{-1}\right) \\ &\quad + \gamma w(x-a)\psi(a)\left(\lambda + \alpha^{-1}\right). \end{aligned} \tag{46}$$

Setting $x = \pm a$ and noting that $\psi(\pm a)$ have the same sign, we have $\psi(a) = \psi(-a) > 0$ with λ satisfying the quadratic equation

$$\left(\lambda + \alpha^{-1} + \beta\right)(\lambda + 1) = \left(\lambda + \alpha^{-1}\right)(1 + \alpha\beta)\Omega, \tag{47}$$

where

$$\Omega = \frac{w(0)+w(2a)}{w(0)-w(2a)}.$$

and we have substituted for γ using equation (42). It follows that $\lambda = \lambda_\pm$ with

$$\lambda_\pm = \frac{1}{2}\left[\Omega(1+\alpha\beta) - \left(1+\alpha^{-1}+\beta\right)\right] \pm \frac{1}{2}\sqrt{\left[\Omega(1+\alpha\beta) - (1+\alpha^{-1}+\beta)\right]^2 + 4(\Omega-1)\,(\alpha^{-1}+\beta)}. \quad (48)$$

The associated eigenmode corresponds to a pure expansion of the bump.

(iv) $\psi(\pm a) < 0$: In this final case equation (43) becomes

$$(\lambda+1)\psi(x) = \gamma w(x+a)\psi(-a)\frac{1}{1+\alpha\beta} + \gamma w(x-a)\psi(a)\frac{1}{1+\alpha\beta}. \quad (49)$$

Setting $x = \pm a$ shows that $\psi(a) = \psi(-a)$ and $\lambda = \lambda_0$ with

$$\lambda_0 = \Omega - 1. \quad (50)$$

The associated eigenmode corresponds to a pure contraction of the bump.

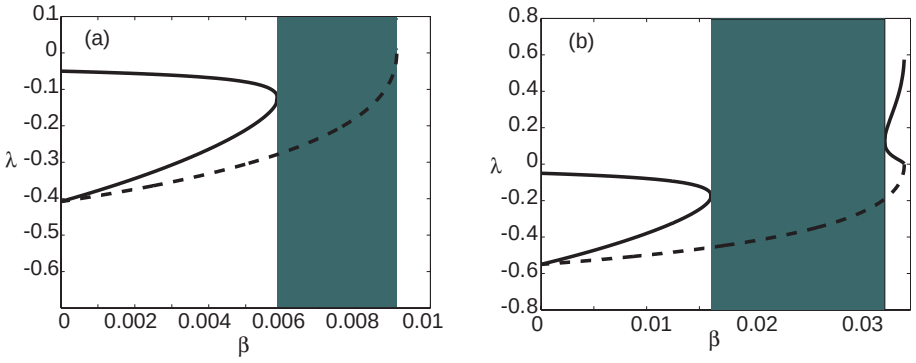

FIGURE 6. Stability with respect to expansion and contraction perturbations (cases (iii) and (iv)). (a) Eigenvalues of the expansion (solid curves) and contraction (dashed curve) perturbations when (a) $\theta = 0.1$ and (b) $\theta = 0.07$. In the grey regions, the roots of equation (48) are complex thus violating the ansatz. Other parameters are $A = 0.6$, $\sigma = 4$, and $\alpha = 0.1$.

We now illustrate an application of the above stability analysis by considering stationary bumps in a network with the Mexican hat weight function (29). Specifically, we plot the spectrum for each type of perturbation in the case of the wider bump shown in Figure 3, which is stable as $\beta \to 0$. In Figure 5, we plot the nonzero eigenvalue λ for shift perturbations; the other two non–zero solutions to the characteristic equation (45) violate the shift restriction $\psi(a) < 0 < \psi(-a)$. As β increases, the eigenvalue becomes positive, representing destabilization through a saddle-node bifurcation, and the perturbation leads to a shift/expansion of the bump, according to the ratio $\Psi(a) \equiv \psi(\pm a)/\psi(\mp a)$. In comparison, the eigenvalues of type (iii) and (iv) perturbations (expansions and contractions) are plotted in Figure 6. As β is increased, the eigenvalues of the expansion perturbation become positive, whereas the contraction perturbation is always stable for the chosen parameters. Since the

expansion instability occurs at larger values of β than shift perturbations, the latter appear to dominate bump instabilities in the case of the given Mexican hat weight function. Another important point is that there exists a parameter range where the roots of the characteristic equation (48) are complex, so stability of expanding perturbations cannot be analyzed using our given ansatz. When real roots appear again, there is a jump in their value. We summarize our stability results in Figure 7, which shows the parameter space (α,β) divided into separate stability regions where either: no bumps exist (black); stable bumps exist (dark grey); unstable bumps exist (light grey); or stability analysis of expansion breaks down (white). Even when the stability analysis of the expansion mode breaks down, bumps destabilize under shift perturbations. Thus, over a physiological range of parameters, if depression is sufficiently weak, bumps remain stable. On the other hand, for strong enough depression, they destabilize via shift perturbations to traveling pulses, as we will show below. The fact that depression reduces the impact of lateral inhibition here leads to inevitable bump destabilization for large enough β.

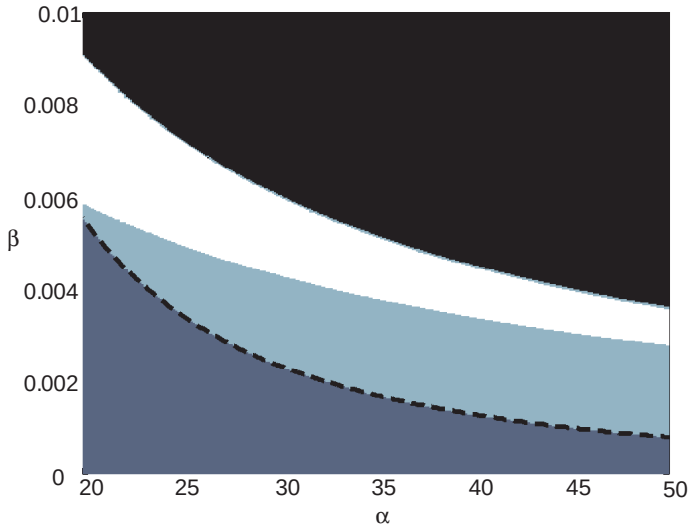

FIGURE 7. Stability map in (α,β) parameter space. Black denotes nonexistence of bumps; light grey denotes unstable bumps; dark grey denotes stable bumps; and white denotes stability analysis of expansions being inconclusive. Dashed black line denotes location of a saddle bifurcation, where stable bumps transition to traveling pulses. Even in the white region, bumps are unstable, due to instability of shift perturbations. Other parameters are $A = 0.6$, $\sigma = 4$, and $\theta = 0.1$.

3.4. **Numerical simulations.** We now study the full system (6) using a numerical approximation scheme. To evolve the system in time, we use a fourth order Runge-Kutta method with 2000-4000 spatial grid points and a time-step of $dt = 0.01$. The integral term in equation (6a) is approximated using Simpson's rule. We systematically examined whether taking finer grids changed stability results, and it does

not. This is important because too coarse a grid can drastically alter numerical results, since discreteness can stabilize bumps that are not stable in the continuous system [33]. For all of our numerical simulations, we begin with an initial condition specified by an associated bump solution (30) that lies on the unstable part of the upper branch of the existence curves shown in Figure 3. After a brief period, we stimulate the system by adding an input perturbation of $u(x,t)$ defined as

$$\psi_{\pm}(x,t) = \chi(t)(w(x+a) \pm w(x-a)), \tag{51}$$

which is motivated by eigenmodes of the linearized Amari equation (1). Leftward shifts (rightward shifts) correspond to $\psi_{-}(x,t)$ when $\chi(t) \geq 0$ ($\chi(t) \leq 0$), while expansions (contractions) correspond to $\psi_{+}(x,t)$ when $\chi(t) \geq 0$ ($\chi(t) \leq 0$). The resulting dynamics depends specifically on the type of perturbation applied to the bump.

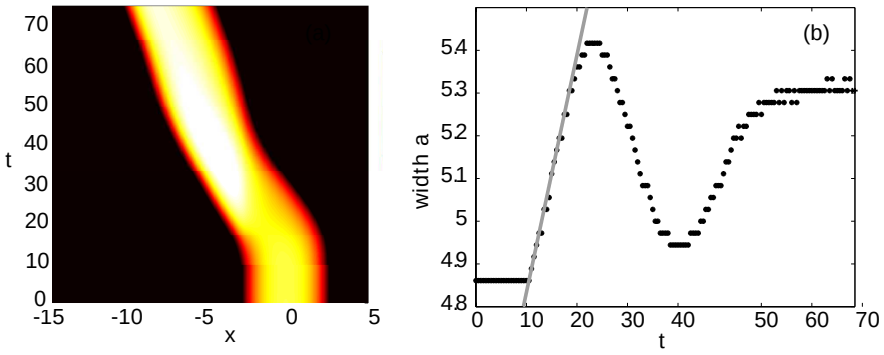

FIGURE 8. Numerical simulation of a bump destabilized by a leftward shift perturbation. (a) Plot of $u(x,t)$ for an initial condition taken to be a stationary bump specified by equation (30). Solution is perturbed at $t = 10$ by a leftward shift $\psi_{-}(x,t)$, such that $\chi(t) = -0.1$ for $t \in [10, 10.1]$ and zero otherwise. (b) Bump width plotted versus time. Bump width increases linearly following the perturbation, but eventually relaxes back to a constant value as the solution evolves to a traveling pulse. Parameters are $A = 0.3$, $\sigma = 4$, $\alpha = 50$, $\beta = 0.01$, $\theta = 0.1$.

When shift perturbations destabilize a bump, the resulting dynamics evolves to a traveling pulse solution. As we showed in previous work, synaptic depression is a reliable mechanism for generating traveling pulses in excitatory neural fields [27, 28]. As illustrated in Figure 8, following a perturbation by a leftward shift, the bump initially expands and then starts to propagate. Eventually, the traveling pulse's width stabilizes to a constant value, larger than the initial bump width. The initial linear growth in the bump's width is consistent with our linear stability calculations. In other simulations, we found that as synaptic depression strength β is increased, the rate of linear growth in the width increases as well, which is also predicted by our stability analysis. In Figure 9, we show an example of how expansions destabilize the bump to result in two counterpropagating pulses. A closer look at the solution as a function of time immediately after the perturbation shows a transient phase, where the superthreshold region is still a connected domain,

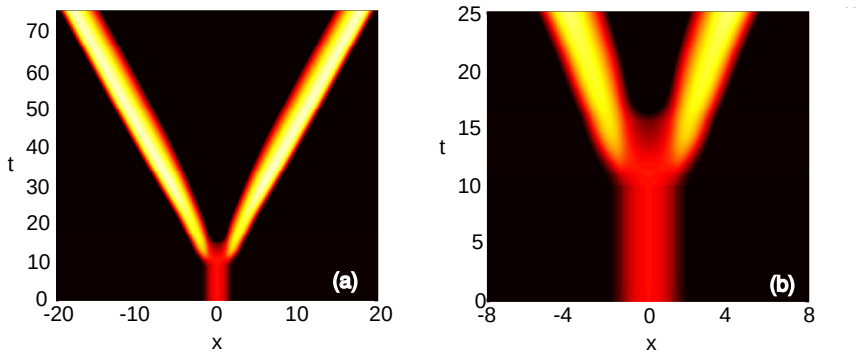

FIGURE 9. Numerical simulation of a bump destabilized by an expanding perturbation. (a) Plot of $u(x,t)$ for an initial condition taken to be stationary bump specified by (30). Solution is perturbed at $t = 10$ by an expansion $\psi_+(x,t)$, such that $\chi(t) = 0.1$ for $t \in [10, 10.1]$ and zero otherwise. (b) Plot of $u(x,t)$ for $t = 0$ to $t = 25$, showing initial expansion of the bump prior to splitting into two counterpropagating pulses. Parameters are $A = 0.3$, $\sigma = 4$, $\alpha = 50$, $\beta = 0.05$, $\theta = 0.1$.

prior to the splitting into two pulses. As also predicted by our stability analysis, we found that contraction perturbations did not drive the system to the homogeneous zero state, unless their amplitude was large enough to drive the system to the other side of the separatrix given by the smaller unstable bump (see Figure 3).

In summary, our mathematical and numerical analysis of stationary bumps in the one-dimensional piecewise smooth neural field model (6) reveals several novel features compared to previous neural field models [2, 7, 5]. These are consequence of the piecewise nature of the linear operator obtained by expanding about the stationary solution. First, shift perturbations that destabilize the bump are a combination of a pure shift and an expansion, rather than a pure shift, leading to an initial increase in the width of the bump prior to propagation as a traveling pulse. Second, there is an asymmetry between expansion and contraction modes, which have different spectra. Physically, this can be understood from the fact that neural populations just outside of the initial bump have maximal synaptic resources so they can recruit their nearest neighbors to continue spreading activity brought about by an initial expansion. On the other hand, neural populations within the interior of the bump do not possess the resources to continue the damping of activity via lateral inhibition brought about by an initial contraction. Finally, note that analyzing stability by formally Taylor expanding equation (6) about a bump solution and prescribing $Q(x)$ on the bump boundary generates stability conditions that underestimate the effectiveness of synaptic depression in destabilizing a bump [27], since they do not take proper account of the piecewise smooth nature of the dynamics.

4. **Two-dimensional bumps.** We now extend our analysis of stationary bumps in a one-dimensional network to derive conditions for the existence and stability of radially symmetric stationary bump solutions of the corresponding two–dimensional

piecewise smooth neural field model

$$\tau \frac{\partial u(\mathbf{r},t)}{\partial t} = -u(\mathbf{r},t) + \int_{\mathbb{R}^2} q(\mathbf{r}',t) w(|\mathbf{r}-\mathbf{r}'|) H(u(\mathbf{r}',t)-\kappa) \mathrm{d}\mathbf{r}', \tag{52a}$$

$$\frac{\partial q(\mathbf{r},t)}{\partial t} = \frac{1-q(\mathbf{r},t)}{\alpha} - \beta q(\mathbf{r},t) H(u(\mathbf{r},t)-\kappa), \tag{52b}$$

where $\mathbf{r} = (r,\phi) \in \mathbb{R}^2$ and $|\mathbf{r}-\mathbf{r}'|$ denotes Euclidean distance in the plane.

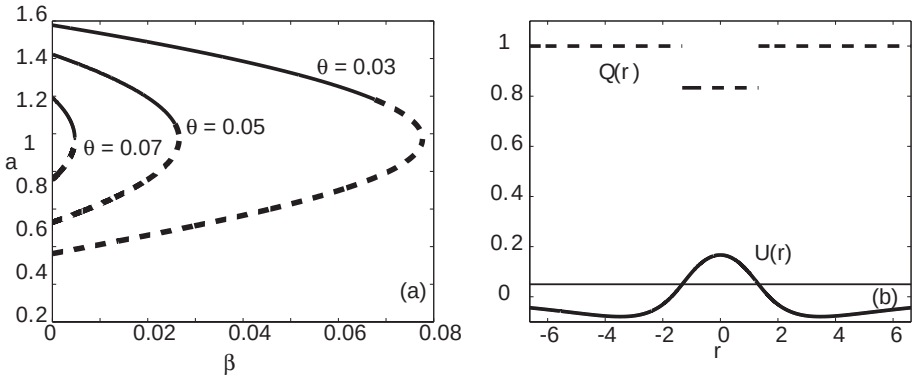

FIGURE 10. Two–dimensional bumps. (a) Plots relating bump radius a to amplitude of synaptic depression β for various values of threshold θ based on equation (63). Solid (dashed) curves indicate bumps that are (stable) unstable with respect to radially symmetric perturbations. Other parameters are $A = 0.3$, $\sigma = 4$, $\alpha = 20$. (b) Bump profile when $\theta = 0.05$, $\alpha = 20$, $\beta = 0.01$.

4.1. **Existence.** Consider a circularly symmetric bump solution of radius a such that $u(\mathbf{r},t) = U(r)$, $q(\mathbf{r},t) = Q(r)$ with $U(a) = \theta$ and

$$U(r) \gtrless \theta, \qquad \text{for } r \lessgtr a, \tag{53}$$

$$\{U(r), Q(r))\} \to \{0,1\}, \qquad \text{as } r \to \infty. \tag{54}$$

Imposing such constraints on a stationary solution of equation (52) gives

$$U(r) = \int_{\mathcal{U}} Q(r') w(|\mathbf{r}-\mathbf{r}'|) \mathrm{d}\mathbf{r}', \tag{55}$$

$$Q(r) = (1+\alpha\beta H(a-r))^{-1}, \tag{56}$$

where $\mathcal{U} = \{\mathbf{r} = (r,\phi) : r \le a\}$ is the domain on which the bump is superthreshold. Substituting equation (56) back into (55) yields

$$(1+\alpha\beta) U(r) = \Pi(a,r), \tag{57}$$

where

$$\Pi(a,r) = \int_0^{2\pi} \int_0^a w(|\mathbf{r}-\mathbf{r}'|) r' \mathrm{d}r' \mathrm{d}\phi'. \tag{58}$$

We can calculate the double integral in (58) using the Hankel transform and Bessel function identities, as in [20, 34]. Thus, we find that

$$\Pi(a,r) = 2\pi a \int_0^\infty \hat{w}(\rho) J_0(r\rho) J_1(a\rho) \mathrm{d}\rho, \tag{59}$$

where $\hat{w}(\rho)$ is the Hankel transform of w.

For the sake of illustration consider a Mexican hat weight distribution given by a combination of modified Bessel functions of the second kind [20, 35, 34]:

$$w(r) = \frac{2}{3\pi}\left(K_0(r) - K_0(2r) - A(K_0(r/\sigma) - K_0(2r/\sigma))\right). \tag{60}$$

Such a weight function is qualitatively similar to a difference of exponential weight functions $w(r) = (2\pi)^{-1}(\mathrm{e}^{-r} - A\mathrm{e}^{-r/\sigma})$. Moreover, following previous studies of two–dimensional neural field models [17, 35, 24, 34, 28], we can transform the system (52) into a fourth order PDE, which is computationally less expensive to evaluate. Using the fact that the corresponding Hankel transform of $K_0(sr)$ is $\mathcal{H}(\rho, s) = (\rho^2 + s^2)^{-1}$, we have

$$\widehat{w}(\rho) = \frac{2}{3\pi}(\mathcal{H}(\rho, 1) - \mathcal{H}(\rho, 2) - A(\mathcal{H}(\rho, 1/\sigma) - \mathcal{H}(\rho, 2/\sigma))). \tag{61}$$

Thus, the integral (59) can be evaluated explicitly by substituting (61) into (59), and using the identity

$$\int_0^\infty \frac{1}{\rho^2 + s^2} J_0(r\rho)J_1(a\rho)\mathrm{d}\rho \equiv \mathcal{I}(a, r, s) = \begin{cases} \frac{1}{s}I_1(sa)K_0(sr), & r > a, \\ \frac{1}{as^2} - \frac{1}{s}I_0(sr)K_1(sa), & r < a, \end{cases}$$

where I_ν is the modified Bessel function of the first kind of order ν. Thus, the stationary bump $U(r)$ given by equation (57) has the form

$$U(r) = \frac{4a}{3(1 + \alpha\beta)}\left(\mathcal{I}(a, r, 1) - \mathcal{I}(a, r, 2) - A(\mathcal{I}(a, r, 1/\sigma) - \mathcal{I}(a, r, 2/\sigma))\right) \tag{62}$$

The bump radius may then be computed by finding the roots a of the equation

$$(1 + \alpha\beta)\theta = \mathbf{\Pi}(a), \tag{63}$$

with

$$\begin{aligned} \mathbf{\Pi}(a) \equiv \Pi(a, a) = \frac{4a}{3}\Big(& I_1(a)K_0(a) - \frac{1}{2}I_1(2a)K_0(2a) \\ & - A(\sigma I_1(a/\sigma)K_0(a/\sigma) - \frac{\sigma}{2}I_1(2a/\sigma)K_0(2a/\sigma))\Big). \end{aligned} \tag{64}$$

Relations between bump radius a and depression strength β are shown in Figure 10 for different thresholds θ.

4.2. **Stability.** We now analyze the stability of radially symmetric two–dimensional bump solutions. As in the case of one–dimensional bumps, we must consider the sign of the perturbations of the bump boundary. However, there are now an infinite number of cases to consider with regard to how perturbations subdivide the continuum boundary of a two–dimensional bump. For this initial exposition, we explicitly compute stability with respect to radially symmetric perturbations only. We also formulate the spectral problem associated with radially nonsymmetric perturbations, but due to its complexity, leave its analysis for future work.

Let us set $u(\mathbf{r}, t) = U(r) + \psi(\mathbf{r}, t)$ and $q(\mathbf{r}, t) = Q(r) + \varphi(\mathbf{r}, t)$. Substituting into the full two-dimensional system (52) and imposing the stationary bump solutions

(55) and (56) gives

$$\begin{aligned}\frac{\partial\psi(\mathbf{r},t)}{\partial t} &= -\psi(\mathbf{r},t) \\ &\quad + \int_{\mathbb{R}^2} w(|\mathbf{r}-\mathbf{r}'|)Q(r')[H(U(r')+\psi(\mathbf{r}',t)-\theta)-H(U(r')-\theta)]\mathrm{d}\mathbf{r}' \\ &\quad + \int_{\mathbb{R}^2} w(|\mathbf{r}-\mathbf{r}'|)\varphi(\mathbf{r}',t)H(U(r')+\psi(\mathbf{r}',t)-\theta)\mathrm{d}\mathbf{r}' \qquad (65)\\ \frac{\partial\varphi(\mathbf{r},t)}{\partial t} &= -\frac{\varphi(\mathbf{r},t)}{\alpha} - \beta Q(r)[H(U(r)+\psi(\mathbf{r},t)-\theta)-H(U(r)-\theta)] \\ &\quad - \beta\varphi(\mathbf{r},t)H(U(r)+\psi(\mathbf{r},t)-\theta). \qquad (66)\end{aligned}$$

In general, perturbations to the bump boundary alter the threshold equation as

$$u(a+\Delta(\phi,t),\phi,t)=\theta$$

for $\phi\in[0,2\pi)$ and all $t>0$. Motivated by this, we introduce the modified field

$$\Phi(\mathbf{r},t) = \int_0^{2\pi}\int_0^{a+\Delta(\phi',t)} w(|\mathbf{r}-\mathbf{r}'|)\varphi(\mathbf{r}',t)\mathrm{d}r'\mathrm{d}\phi', \qquad (67)$$

and convolving equation (66) with the weight function $w(r)$ over the domain with boundary $r=a+\Delta(\phi,t)$ for $\phi\in[0,2\pi)$ gives

$$\begin{aligned}\frac{\partial\psi(\mathbf{r},t)}{\partial t} &= -\psi(\mathbf{r},t)+\Phi(\mathbf{r},t)+\int_0^{2\pi}\int_0^{a+\Delta(\phi',t)} w(|\mathbf{r}-\mathbf{r}'|)Q(r')r'\mathrm{d}r'\mathrm{d}\phi' \\ &\quad - \int_0^{2\pi}\int_0^{a} w(|\mathbf{r}-\mathbf{r}'|)Q(r')r'\mathrm{d}r'\mathrm{d}\phi' \qquad (68)\\ \frac{\partial\Phi(\mathbf{r},t)}{\partial t} &= -(\alpha^{-1}+\beta)\Phi(\mathbf{r},t) - \beta\int_0^{2\pi}\int_0^{a+\Delta(\phi',t)} w(|\mathbf{r}-\mathbf{r}'|)Q(r') \\ &\quad \times[H(U+\psi-\theta)-H(U-\theta)]r'\mathrm{d}r'\mathrm{d}\phi'. \qquad (69)\end{aligned}$$

We now truncate these equations by retaining only those terms first–order in the perturbations ψ, Φ, Δ. As in the case of one-dimensional bumps, it is important to keep track of the sign of $\Delta(\phi,t)$ at all values of ϕ when approximating the integrals, since $Q(r)$ is discontinuous on the boundary. For example

$$\begin{aligned}\int_0^{2\pi}\int_a^{a+\Delta(\phi',t)} w(|\mathbf{r}-\mathbf{r}'|)Q(r')r'\mathrm{d}r'\mathrm{d}\phi' &\approx a\int_{\mathcal{A}_+(t)}\Delta(\phi',t)w(|\mathbf{r}-\mathbf{a}|)\mathrm{d}\phi' \qquad (70)\\ &\quad + \frac{a}{1+\alpha\beta}\int_{\mathcal{A}_-(t)}\Delta(\phi',t)w(|\mathbf{r}-\mathbf{a}|)\mathrm{d}\phi',\end{aligned}$$

where the domain $\mathcal{A}_+(t)$ ($\mathcal{A}_-(t)$) defines the region in ϕ over which the perturbation $\psi(a,\phi,t)>0$ ($\psi(a,\phi,t)<0$) at time $t>0$ and $\mathbf{a}=(a,\phi')$. Likewise, the integral on the right hand side of (69) can be approximated by

$$a\int_{\mathcal{A}_+}\Delta(\phi',t)w(|\mathbf{r}-\mathbf{a}|)\mathrm{d}\phi'. \qquad (71)$$

Finally, we use the approximation

$$\begin{aligned}\theta &= u(a+\Delta(\phi,t),\phi,t)=U(a+\Delta(\phi,t))+\psi(a+\Delta(\phi,t),\phi,t), \\ &\approx U(a)+U'(a)\Delta(\phi,t)+\psi(a,\phi),\end{aligned}$$

and $U(a)=\theta$ so that

$$\Delta(\phi,t) \approx \frac{\psi(a,\phi,t)}{|U'(a)|}$$

to first order, then we obtain the following set of equations

$$\begin{aligned}\frac{\partial \psi(\mathbf{r},t)}{\partial t} &= -\psi(\mathbf{r},t)+\Phi(\mathbf{r},t)+a\gamma\int_{\mathcal{A}_+(t)}\psi(a,\phi',t)w(|\mathbf{r}-\mathbf{a}|)\mathrm{d}\phi' \\ &\quad +\frac{a\gamma}{1+\alpha\beta}\int_{\mathcal{A}_-(t)}\psi(a,\phi',t)w(|\mathbf{r}-\mathbf{a}|)\mathrm{d}\phi', \qquad (72)\\ \frac{\partial \Phi(\mathbf{r},t)}{\partial t} &= -(\alpha^{-1}+\beta)\Phi(\mathbf{r},t)-a\gamma\beta\int_{\mathcal{A}_+(t)}\psi(a,\phi',t)w(|\mathbf{r}-\mathbf{a}|)\mathrm{d}\phi'. \qquad (73)\end{aligned}$$

Here

$$\gamma^{-1} = |U'(a)| = \frac{2\pi a}{1+\alpha\beta}\int_0^\infty \rho\widehat{w}(\rho)J_1(a\rho)J_1(a\rho)\mathrm{d}\rho, \qquad (74)$$

which for the Mexican hat weight function (60) can be explicitly computed as

$$\begin{aligned}|U'(a)| &= \frac{4a}{3(1+\alpha\beta)}\left(I_1(a)K_1(a)-I_1(2a)K_1(2a)\right. \qquad (75)\\ &\quad \left.-A(I_1(a/\sigma)K_1(a/\sigma)-I_1(2a/\sigma)K_1(2a/\sigma))\right).\end{aligned}$$

Equations (72) and (73) imply that the local stability of a stationary bump solution depends on the spectral properties of a piecewise linear operator. As in the one-dimensional case, we can obtain a simpler spectral problem under the ansatz that the perturbation $\psi(a,\phi,t)$ (equivalently $\Delta(\phi,t)$) does not switch sign at each ϕ for any time t. Thus, we assume (72) and (73) have separable solutions $(\psi(\mathbf{r},t),\Phi(\mathbf{r},t))=\mathrm{e}^{\lambda t}(\psi(\mathbf{r}),\Phi(\mathbf{r}))$, where λ is real. Under this assumption, the domains $\mathcal{A}_\pm(t)$ are constant in time, so there is a common factor $\mathrm{e}^{\lambda t}$ that cancels everywhere. We thus obtain an eigenvalue equation for λ of the form

$$\begin{aligned}(\lambda+1)\psi(\mathbf{r}) &= \frac{a\gamma(\lambda+\alpha^{-1})}{\lambda+\alpha^{-1}+\beta}\int_{\mathcal{A}_+}\psi(a,\phi')w(|\mathbf{r}-\mathbf{a}|)\mathrm{d}\phi' \qquad (76)\\ &\quad +\frac{a\gamma}{1+\alpha\beta}\int_{\mathcal{A}_-}\psi(a,\phi')w(|\mathbf{r}-\mathbf{a}|)\mathrm{d}\phi'.\end{aligned}$$

One class of solutions to equation (76) consists of functions $\psi(\mathbf{r})$ that vanish on the boundary, $\psi(a,\phi)=0$, such that $\lambda=-1$. This determines the essential spectrum, since $\lambda=-1$ has infinite multiplicity, and does not contribute to any instabilities. Otherwise, $\psi(r,\phi)$ is determined entirely by its values $\psi(a,\phi)$ on the restricted domain $r=a$. Hence, we need only consider $r=a$, which yields the integral equation

$$\begin{aligned}(\lambda+1)\psi(a,\phi) &= \frac{a\gamma(\lambda+\alpha^{-1})}{\lambda+\alpha^{-1}+\beta}\int_{\mathcal{A}_+}\psi(a,\phi')w\left(2a\sin\frac{\phi-\phi'}{2}\right)\mathrm{d}\phi' \qquad (77)\\ &\quad +\frac{a\gamma}{1+\alpha\beta}\int_{\mathcal{A}_-}\psi(a,\phi')w\left(2a\sin\frac{\phi-\phi'}{2}\right)\mathrm{d}\phi',\end{aligned}$$

where we have simplified the argument of $w(r)$ using

$$|(a,\phi)-(a,\phi')|=\sqrt{(a\sin\phi-a\sin\phi')^2+(a\cos\phi-a\cos\phi')^2}=2a\sin\frac{\phi-\phi'}{2}.$$

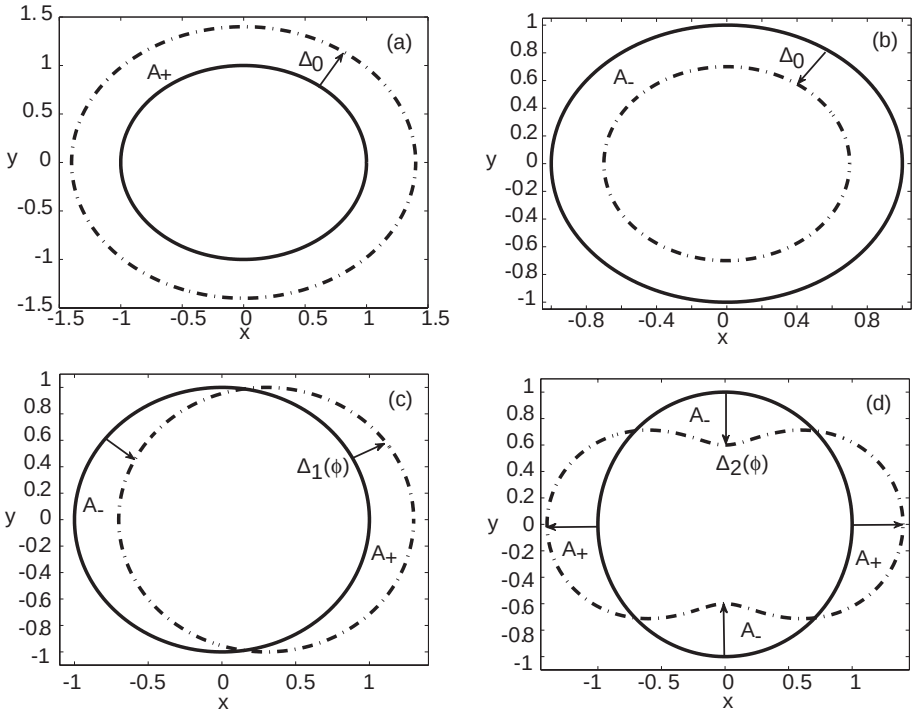

FIGURE 11. Low-order perturbations of a radially symmetric two–dimensional bump. (a) expansion ($\Delta_0 > 0$); (b) contraction ($\Delta_0 < 0$); (c) D_1-symmetric shift $\Delta_1(\phi)$; (d) D_2-symmetric perturbation $\Delta_2(\phi)$

There are then three other classes of solution to equation (77): (i) radially symmetric expansions, such that $\psi(a,\phi) = \psi(a) > 0$ for $\phi \in [0, 2\pi)$; (ii) radially symmetric contractions, such that $\psi(a,\phi) = \psi(a) < 0$ for $\phi \in [0, 2\pi)$; and (iii) radially non-symmetric perturbations for which $\psi(a,\phi)$ changes sign as a function of ϕ. In the limit $\beta \to 0$, equation (77) reduces to the simpler form

$$(\lambda+1)\psi(a,\phi) = a\gamma \int_0^{2\pi} \psi(a,\phi')w\left(2a\sin\frac{\phi-\phi'}{2}\right)\mathrm{d}\phi'. \tag{78}$$

The eigenmodes are then given by pure Fourier modes $\psi(a,\phi) = \Delta_n(\phi) \equiv c_n \mathrm{e}^{in\phi} +$ c.c., integer n, with corresponding real eigenvalues $\lambda_n = -1 + \gamma\mu_n$,

$$\mu_n = 2a \int_0^{2\pi} w(2a\sin\phi)\mathrm{e}^{-2in\phi}d\phi. \tag{79}$$

Some examples of low–order Fourier eigenmodes $\Delta_n(\phi)$ are shown in Figure 11, together with the associated boundary domains $\mathcal{A}_\pm$. As β is increased from zero only the zeroth-order eigenmodes persist (expansions and contractions), whereas the non-radially symmetric eigenmodes become a mixture of Fourier modes:

$$\psi(a,\phi) = \sum_{n=-\infty}^{\infty} c_n(a)\mathrm{e}^{in\phi}.$$

This is analogous to the mixing between shift and expansion perturbations in the one–dimensional case.

(i) $\psi(a,\phi)=\psi(a)>0$: In this case, equation (77) becomes

$$(\lambda+1)\psi(a) = \frac{a\gamma(\lambda+\alpha^{-1})\psi(a)}{\lambda+\alpha^{-1}+\beta}\int_0^{2\pi} w\left(2a\sin\frac{\phi-\phi'}{2}\right)\mathrm{d}\phi', \tag{80}$$

where we have used the facts that $\mathcal{A}_+ = [0,2\pi)$, $\mathcal{A}_-$ is empty, and $\psi(a,\phi)$ is constant in ϕ. Therefore, the right–hand side of equation (80) is independent of ϕ and λ satisfies the quadratic

$$(\lambda+\alpha^{-1}+\beta)(\lambda+1) = (\lambda+\alpha^{-1})(1+\alpha\beta)\Omega_0, \tag{81}$$

where

$$\Omega_0=\frac{\mu_0(a)}{(1+\alpha\beta)|U'(a)|},\qquad \mu_0(a)=2a\int_0^{\pi} w(2a\sin\phi)\mathrm{d}\phi. \tag{82}$$

For the Mexican hat weight function (60), we can use

$$\int_0^{\pi} K_0(2b\sin\phi)\mathrm{d}\phi = \pi I_0(b)K_0(b)$$

to calculate

$$\begin{aligned}\mu_0(a) = {}& \frac{4a}{3}(I_0(a)K_0(a)-I_0(2a)K_0(2a) \\ & -A(I_0(a/\sigma)K_0(a/\sigma)-I_0(2a/\sigma)K_0(2a/\sigma))).\end{aligned} \tag{83}$$

It follows that $\lambda=\lambda_0^{\pm}$ with

$$\begin{aligned}\lambda_0^{\pm} = {}& \frac{1}{2}\left[\Omega_0(1+\alpha\beta)-(1+\alpha^{-1}+\beta)\right] \\ & \pm\frac{1}{2}\sqrt{[\Omega_0(1+\alpha\beta)-(1+\alpha^{-1}+\beta)]^2+4(\Omega_0-1)(\alpha^{-1}+\beta)}.\end{aligned} \tag{84}$$

The associated eigenmode corresponds to pure expansion of the bump.

(ii) $\psi(a,\phi)=\psi(a)<0$: In this case, equation (77) becomes

$$(\lambda+1)\psi(a) = \frac{a\gamma\psi(a)}{1+\alpha\beta}\int_0^{2\pi} w\left(2a\sin\frac{\phi-\phi'}{2}\right)\mathrm{d}\phi', \tag{85}$$

where we have used the facts that $\mathcal{A}_+$ is empty, $\mathcal{A}_- = [0,2\pi)$, and $\psi(a,\phi)$ is constant in ϕ. Therefore, the right–hand side of equation (85) is independent of ϕ and $\lambda=\lambda_0$ with

$$\lambda_0 = \Omega_0-1. \tag{86}$$

The associated eigenmode corresponds to pure contraction of the bump.

(iii) $\psi(a,\phi)$ radially non-symmetric : In this final case for $\beta>0$, the characteristic equations (77) involves integrals over subdomains of $[0,2\pi)$, and is no longer a standard Fredholm integral equation. Hence, as we have already indicated, eigenmodes will be more complicated than the pure Fourier modes $\mathrm{e}^{in\phi}$ found in previous studies of bump instabilities in two-dimensions [17, 20, 21, 34]. This is due to the faster growth of the lobes of the perturbation $\psi(a,\phi)$ that are superthreshold versus those that are subthreshold. We leave the explicit analysis of general solutions of equation (77) to future work.

We illustrate the stability properties of two–dimensional bumps with respect to radially symmetric perturbations by plotting the spectrum of expansions and contractions in the case of the Mexican hat weight function (60), see Figure 12. We

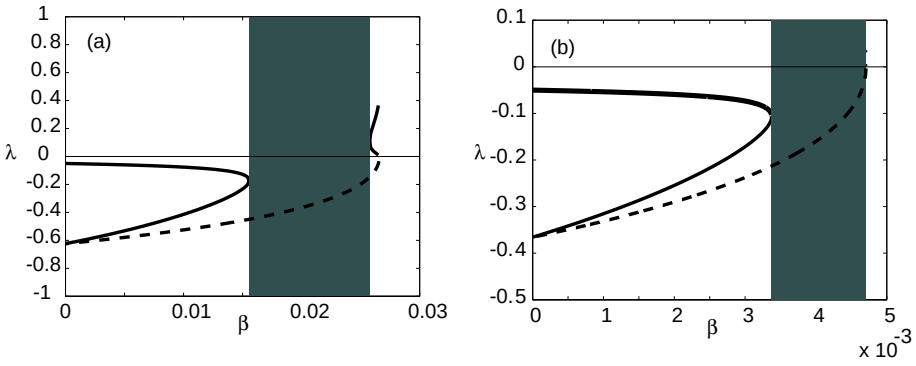

FIGURE 12. Stability of a two–dimensional bump with respect to radially symmetric perturbations. Eigenvalues of the expansion (solid curves) and contraction (dashed curve) perturbations are plotted for (a) $\theta = 0.05$ and (b) $\theta = 0.07$. Stability analysis of expansion perturbations breaks down in the grey region due to the roots (84) being complex. Other parameters are $A = 0.3$, $\sigma = 4$, and $\alpha = 20$.

consider the upper branches of the existence curves shown in Figure 10, since these are stable in the limit $\beta \to 0$. As in the one-dimensional case, the expansion mode dominates over contraction, due to more resources existing outside of the bump. As β increases, the two roots of the characteristic equation (84) meet and they become complex, violating our ansatz. When the eigenvalues become real again, they are both greater than zero, implying the bump will certainly be unstable. Contraction perturbations are always stable. By analogy with one–dimensional bumps, we expect that bump instabilities in two dimensions are dominated by higher-order perturbations of the bump boundary that include shifts, see Figure 11.

5. **Discussion.** In this paper, we analyzed the existence and stability of stationary bumps in a one–dimensional piecewise smooth neural field model with synaptic depression. We showed that the local stability of a bump is determined by the spectrum of a piecewise linear operator that keeps track of the sign of perturbations of the bump boundary. For concreteness, we considered a Mexican hat weight function such that for sufficiently weak synaptic depression ($\beta \to 0$), a stable bump exists. As β is increased, the bump becomes unstable with respect to perturbations that shift the boundary of the bump, leading to the formation of a traveling pulse. We found two important consequences of the piecewise smooth nature of the dynamics. First, the shift perturbation is a mixture of a pure shift and an expansion, leading to an initial increase in the width of the bump prior to propagation as a traveling pulse. Second, there is an asymmetry between expansion and contraction modes due to more synaptic resources existing outside of the bump. In the final part of the paper, we extended our analysis to the case of radially symmetric two–dimensional bumps and showed how the piecewise smooth dynamics leads to a mixing of Fourier modes associated with perturbations of the circular bump boundary.

In future work, we will explore further consequences of piecewise smooth dynamics in neural field theories. For the particular examples considered in this paper,

the dominant instabilities were associated with real rather than complex eigenvalues, which greatly simplified the analysis. However, there are well known scenarios in neural field models with linear adaptation, where Hopf bifurcations can occur leading to spatially structured oscillations such as breathers and target patterns [8, 20, 21, 24, 25]. It would be interesting to explore generalized Hopf bifurcations in neural field models with nonlinear forms of adaptation such as synaptic depression, along the lines of recent studies of nonsmooth dynamical systems [36, 37]. It is likely that similar issues to those highlighted in this paper will also apply to another class of piecewise smooth neural field model, which includes the effects of nonlinear threshold dynamics [38]. Finally, just as depression is a viable local negative feedback mechanism, facilitation can be used in the same way if it specifically amplifies inhibitory synapses [32, 26]. Thus another extension is to consider a two population model, in which depression acts on excitatory synapses, while facilitation acts on inhibitory synapses. Such a model is suggested by experimental studies of short term synaptic plasticity [39].

Acknowledgements. This publication was based on work supported in part by the National Science Foundation (DMS-0813677) and by Award No KUK-C1-013-4 made by King Abdullah University of Science and Technology (KAUST). PCB was also partially supported by the Royal Society Wolfson Foundation.

REFERENCES

[1] H. R. Wilson and J. D. Cowan. A mathematical theory of the functional dynamics of cortical and thalamic nervous tissue. *Kybernetik* **13**, 55–80 (1973).
[2] S. Amari, Dynamics of pattern formation in lateral-inhibition type neural fields, Biol. Cybern. 27 (2) (1977) 77–87.
[3] G. B. Ermentrout, Neural networks as spatio-temporal pattern forming systems, Rep. Prog. Phys. **61** (1998) 353–430.
[4] P. C. Bressloff, Spontaneous symmetry breaking in self-organizing neural fields, Biol. Cybern. 93(4) (2005) 256–274.
[5] S Coombes. Waves, bumps and patterns in neural field theories. *Biol. Cybern.* 93(2), 91–108 (2005).
[6] J. P. Keener, Waves in excitable media, SIAM J. Appl. Math. 39(3) (1980) 528–548.
[7] D. J. Pinto, G. B. Ermentrout, Spatially structured activity in synaptically coupled neuronal networks: I. Traveling fronts and pulses, SIAM J. Appl. Math. 62 (1) (2001) 206–225.
[8] D. J. Pinto, G. B. Ermentrout, Spatially structured activity in synaptically coupled neuronal networks: II. Lateral inhibition and standing pulses, SIAM J. Appl. Math. 62 (1) (2001) 226–243.
[9] R. D. Chervin, P. A. Pierce, B. W. Connors, Periodicity and directionality in the propagation of epileptiform discharges across neocortex, J Neurophysiol 60 (5) (1988) 1695–1713.
[10] J.-Y. Wu, L. Guan, Y. Tsau, Propagating activation during oscillations and evoked responses in neocortical slices, J Neurosci. 19 (12) (1999) 5005–5015.
[11] J.-Y. Wu, Propagating waves of activity in the neocortex: what they are, what they do, Neuroscientist 14 (5) (2008) 487–502.
[12] X-J Wang. Synaptic reverberation underlying mnemonic persistent activity. *Trends Neurosci.*, 24:455–463, 2001.
[13] S. Coombes, M. R. Owen, Evans functions for integral neural field equations with Heaviside firing rate function, 3(4) (2004) 574–600.
[14] K Kishimoto and S Amari. Existence and stability of local excitations in homogeneous neural fields. *J. Math. Biol.*, 7:303–318, 1979.
[15] O. Faugeras, R. Veltz, F. Grimbert, Persistent neural states: Stationary localized activity patterns in nonlinear continuous n-population, q-dimensional neural networks, Neural Comput. 21 (2009) 147–187.
[16] C R Laing, W C Troy, B Gutkin, and G B Ermentrout. Multiple bumps in a neuronal model of working memory. *SIAM J. Appl. Math*, 63:62–97, 2002.

[17] C R Laing and W C Troy. PDE methods for nonlocal models. *SIAM J. Appl. Dyn. Syst.*, 2:487–516, 2003.
[18] Z. P. Kilpatrick, S. E. Folias and P. C. Bressloff. Traveling pulses and wave propagation failure in an inhomogeneous neural network. *SIAM J. Appl. Dyn. Syst.* **7** 161-185 (2008).
[19] H Werner and T Richter. Circular stationary solutions in two-dimensional neural fields. *Biol. Cybern.*, 85:211–217, 2001.
[20] S. E. Folias, P. C. Bressloff, Breathing pulses in an excitatory neural network, SIAM J. Appl. Dyn. Syst. 3 (3) (2004) 378–407.
[21] S. E. Folias, P. C. Bressloff, Breathers in two-dimensional neural media, Phys. Rev. Lett. 95 (20) (2005) 208107.
[22] P C Bressloff. Weakly interacting pulses in synaptically coupled excitable neural media. *SIAM J. Appl. Math.*, 66:57–81, 2005.
[23] R. Fitzhugh, Impulses and physiological states in theoretical models of nerve membrane, Biophys. J. 1 (1961) 445-466.
[24] W. C. Troy, V. Shusterman, Patterns and features of families of traveling waves in large-scale neuronal networks, SIAM J. Appl. Dyn. Syst. 6 (2007) 263–292.
[25] V. Shusterman, W. C. Troy, From baseline to epileptiform activity: a path to synchronized rhythmicity in large-scale neural networks, Phys. Rev. E 77 (2008) 061911.
[26] R. S. Zucker, W. G. Regehr, Short–term synaptic plasticity, Ann. Rev. Physiol. 64 (2) (2002) 355–405.
[27] Z. P. Kilpatrick, P. C. Bressloff, Effects of synaptic depression and adaptation on spatiotemporal dynamics of an excitatory neuronal network, Physica D (2009) in press.
[28] Z. P. Kilpatrick, P. C. Bressloff, Spatially structured oscillations in a two-dimensional excitatory neuronal network with synaptic depression, J. Comput. Neurosci. (2009) in press.
[29] M. Tsodyks, K. Pawelzik, H. Markram, Neural networks with dynamic synapses, Neural Comput. 10 (4) (1998) 821–835.
[30] J. Tabak, W. Senn, M. J. O'Donovan, J. Rinzel, Modeling of spontaneous activity in developing spinal cord using activity-dependent depression in an excitatory network, J Neurosci. 20 (8) (2000) 3041–3056.
[31] L. F. Abbott, J. A. Varela, K. Sen, S. B. Nelson, Synaptic depression and cortical gain control., Science 275 (5297) (1997) 220–224.
[32] M. V. Tsodyks, H. Markram, The neural code between neocortical pyramidal neurons depends on neurotransmitter release probability, Proc. Natl. Acad. Sci. USA 94 (2) (1997) 719–723.
[33] Y. Guo, C. C. Chow, Existence and stability of standing pulses in neural networks: II. Stability, SIAM J. Appl. Dyn. Syst. 4 (2) (2005) 249–281.
[34] M. R. Owen, C. R. Laing, S. Coombes, Bumps and rings in a two-dimensional neural field: splitting and rotational instabilities, New Journal of Physics 9 (2007) 378.
[35] C.R. Laing, Spiral waves in nonlocal equations. SIAM J Appl. Dyn. Syst. 4 (2005) 588–606.
[36] M. Di Bernardo, C. J. Budd, A. R. Champneys, Bifurcations in Nonsmooth Dynamical Systems, SIAM Rev. 50 (2008) 629-701.
[37] Y. Zou, T. Kupper, W. J. Beyn, Generalized Hopf bifurcation for planar Filippov systems continuous at the origin, J. Nonlinear Sci. 16 (2006) 159-177.
[38] S. Coombes, M. R. Owen, Bumps, breathers, and waves in a neural network with spike frequency adaptation, Phys. Rev. Lett. 94 (14) (2005) 148102.
[39] O. Melamed, O. Barak, G. Silberberg, H. Markram, M. Tsodyks, Slow oscillations in neural networks with facilitating synapses, J. Comput. Neurosci. 25 (2008) 308-316.

E-mail address: `bressloff@maths.ox.ac.uk`

RECENT REPORTS

14/09	Chaste: a test-driven approach to software development for physiological modelling	Pitt-Francis *et al.*
15/09	Block triangular preconditioners for PDE constrained optimization	Rees Stoll
16/09	From microscopic to macroscopic descriptions of cell migration on growing domains	Baker Yates Erban
17/09	The Influence of Gene Expression Time Delays on Gierer-Meinhardt Pattern Formation Systems	Seirin Lee Gaffney Monk
18/09	Analysis of a stochastic chemical system close to a sniper bifurcation of its mean field model	Erban *et al.*
19/09	On the existence and the applications of modified equations for stochastic differential equations	Zygalakis
20/09	Pebble bed: reflector treatment and pressure velocity coupling	Charpin *et al.*
21/09	A finite difference method for free boundary problems	Fornberg
22/09	Tangent unit-vector fields: nonabelian homotopy invariants and the Dirichlet energy	Majumdar Robbins Zyskin
23/09	Morphological instability of a nonequilibrium icecolloid interface	Peppin Majumdar Wettlaufer
24/09	The effect of polar lipids on tear film dynamics	Aydemir Breward Witelski
25/09	Preconditioning for active set and projected gradient methods as semi-smooth Newton methods for PDE-constrained optimization with control constraints	Stoll Wathen
26/09	Functional differential equations arising in cell-growth	Wake Begg
27/09	A Cell Growth Model Revisited	Derfel van Brunt Wake
28/09	Quasi-steady state reduction of molecular motor-based models of directed intermittent search	Newby Bressloff
29/09	All-at-once preconditioning in PDE-constrained optimization	Rees Stoll Wathen

30/09	An hp-Local Discontinuous Galerkin method for Parabolic Integro-Differential Equations	Pani Yadav
31/09	Stochastic neural field theory and the system-size expansion	Bressloff
32/09	A Hamiltonian Krylov-Schur-type method based on the symplectic Lanczos process	Benner Faßbender Stoll
33/09	Nematic liquid crystals : from Maier-Saupe to a continuum theory	Ball Majumdar
34/09	Tangent unit-vector fields: nonabelian homotopy invariants and the Dirichlet energy	Majumdar Robbins Zyskin
35/09	A metabolite-sensitive, thermodynamically-constrained model of cardiac cross-bridge cycling: Implications for force development during ischemia	Tran Smith Loiselle Crampin
36/09	Modelling bacterial behaviour close to a no-slip plane boundary: the influence of bacterial geometry	Shum Gaffney Smith
37/09	Optimal L2-error estimates for the semidiscrete Galerkin approximation to a second order linear parabolic initial and boundary value problem with nonsmooth initial data	Goswami Pani
38/09	Optimal L2 estimates for semidiscrete Galerkin methods for parabolic integro-differential equations with nonsmooth data	Goswami Pani Yadav
39/09	Spatially structured oscillations in a two-dimensional excitatory neuronal network with synaptic depression	Kilpatrick Bressloff

Copies of these, and any other OCCAM reports can be obtained from:

Oxford Centre for Collaborative Applied Mathematics
Mathematical Institute
24 - 29 St Giles'
Oxford
OX1 3LB
England
www.maths.ox.ac.uk/occam